Journal of Hydrology 466–467 (2012) 73–87

Contents lists available at SciVerse ScienceDirect

Journal of Hydrology

journal homepage: www.elsevier.com/locate/jhydrol

Uncertainty assessment of climate change impacts for hydrologically distinct river basins

Il-Won Jung [a,b,c], H. Moradkhani [a,c,*], H. Chang [b,c]

[a] Department of Civil & Environmental Engineering, Portland State University, 1930 SW 4th Avenue, Suite 200, Portland, OR 97201, USA
[b] Department of Geography, Portland State University, 1721 SW Broadway, Portland, OR 97201, USA
[c] Institute for Sustainable Solutions, Portland State University, Portland, OR 97201, USA

ARTICLE INFO

Article history:
Received 4 February 2010
Received in revised form 26 July 2012
Accepted 4 August 2012
Available online 16 August 2012
This manuscript was handled by Andras Bardossy, Editor-in-Chief, with the assistance of Harald Kunstmann, Associate Editor

Keywords:
Climate change
Uncertainty
Climate change impact assessment
Snowmelt
PRMS

SUMMARY

The hydrologic uncertainty of climate change impacts in two river basins in the Pacific Northwest of US is investigated. One basin is dominated by snowfall in winter, resulting in snowmelt in spring and early summer, and the other basin is dominated by rainfall in all seasons. In addition to hydrologic uncertainties, we consider the combined effect of two emission scenarios and eight general circulation models (GCMs) in our analyses. Latin Hypercube Sampling (LHS) is employed to sample the Precipitation Runoff Modeling System (PRMS) parameter space and the behavioral parameter sets were obtained according to a statistical performance measure. The results suggest that the relative impacts of uncertainties from different sources vary between the two basins. It is shown that changes in winter runoff are more affected by hydrologic model parameter uncertainty in the snow-dominated basin, while they are less influenced in the rain-dominated basin. The differences in the amount and timing of snowmelt as a result of model parameter uncertainty contribute to the variations of change in winter runoff in the snowfall-dominated basin. This result indicates that climate change impact studies for snow-dominated regions require more cautious interpretation of runoff projections due to considerable uncertainty in estimated hydrologic model parameters.

1. Introduction

As the Earth's climate shifts, understanding, quantifying, and reducing uncertainties in hydrologic climate change impact assessments are critical to the development of adaptive water resources management plans. Several studies have attempted to quantify the uncertainty arising from a variety of sources, including future greenhouse gas (GHG) and aerosol emissions, general circulation model (GCM) structure and initial conditions (e.g. Tebaldi et al., 2005; Hawkins and Sutton, 2009), downscaling method (e.g. Wood et al., 2004; Im et al., 2010; Najafi et al., 2011a), and hydrologic model structure and parameters (Wilby and Harris, 2006; Jiang et al., 2007; Prudhomme and Davies, 2008; Kay et al., 2009; Chang and Jung, 2010; Bae et al., 2011; Najafi et al., 2011b).

Wilby and Harris (2006) investigated the uncertainties associated with low-flow change, stemming from a combination of emission scenarios, GCM structures, statistical downscaling methods, and hydrologic model parameters and structure. Their results indicated that the low flow change was most sensitive to uncertainty in the GCM structure and downscaling method, but it was less affected by uncertainties due to hydrological model parameters and emission scenarios. The Intergovernmental Panel on Climate Change (IPCC) Fourth Assessment Report (AR4) also demonstrated that climate projection derived from different GCMs is the biggest source of the uncertainty in projected water resources impacts (Bates et al., 2008). Kay et al. (2009) conducted an uncertainty assessment of flood frequency analysis in England and included two other sources of uncertainty: the GCM initial condition and downscaling method. As part of the change in flood frequency, their results indicated that uncertainties due to GCM initial conditions and RCM structure are more significant if the results from an extreme GCM simulation are excluded. Jung et al. (2011) showed that the uncertainty associated with urban flooding analysis is highly affected by the GCM structure in the shorter term flood frequency change (e.g., 2 and 5 year floods), while the uncertainty is dominated by natural variability in the longer term flood frequency change (above 25 year floods). Moradkhani et al. (2010) developed several procedural elements to address the effect that climate change may have on riparian and floodplain-connected areas and showed the application for a river basin in the Pacific Northwest US.

Jiang et al. (2007) employed six monthly water balance models to assess hydrologic model structural uncertainty. They showed that the selection of hydrologic models results in different

* Corresponding author at: Department of Civil and Environmental Engineering, Institute for Sustainable Solutions, Portland State University, Portland, OR 97201, USA. Tel.: +1 503 725 2436; fax: +1 503 725 5950.
E-mail address: hamidm@cecs.pdx.edu (H. Moradkhani).

0022-1694/$ - see front matter © 2012 Elsevier B.V. All rights reserved.
http://dx.doi.org/10.1016/j.jhydrol.2012.08.002

hydrologic climate change impacts. Najafi et al. (2011b) used four hydrologic models with different levels of complexity to assess climate change impacts. Their results showed that hydrologic model selection is more critical in the dry season than in the wet season in rainfall-dominated regions. Bae et al. (2011) analyzed the effects of semi-distributed model structures and potential evapotranspiration (PET) methods by using PRMS, Soil and Water Assessment Tool (SWAT), and Semi-distributed Land Use based Runoff Processes (SLURP). They reported that the uncertainty from hydrological model and PET is greater in the distant future than in the near future because of the different sensitivity of PET methods to temperature change. In agreement with their study, Madadgar and Moradkhani (in press) reported that more caution is needed for assessing future change in the risk of low flows and droughts because of higher uncertainty in the dry season than the wet season. In addition, Madadgar and Moradkhani (in press) analyzed the joint behavior of drought characteristics under climate change using copula multivariate procedure.

Regional hydrological process is closely related to local geological characteristics and hydroclimatologic attributes. Tague et al. (2008) and Chang and Jung (2010) showed that two geologically different basins, one dominated by High Cascades geology and the other by Western Cascades geology, had significantly different changes in summer runoff under identical climate change conditions. The Western Cascades are composed of low permeability volcanic rocks in a highly dissected landscape with steep topography, which induces a faster discharge to streamflow; the High Cascades, by contrast, have young, permeable volcanic rocks, little dissection, and mild slopes, which creates a deep groundwater system (Tague et al., 2008). Similarly, in two separate studies on English basins, Kay et al. (2009) and Prudhomme and Davies (2008) indicated that major uncertainty sources might vary depending on the locations of the basins with differing hydroclimatology. In addition, uncertainties in climate change impact assessment could vary between basins not just because of basin hydroclimatologic characteristics but due to better or poorer matches between the GCM or RCM simulations and conditions in each region and/or season.

This study aims to compare the uncertainties in climate change impact assessment in two hydrologically distinct basins. The study areas are the Clackamas River Basin (CRB) and the Tualatin River Basin (TRB), sub-basins of the Willamette River Basin in Oregon, USA that have contrasting hydrologic regimes. The two basins are near each other and share the same temperate marine climate characterized by dry summers and wet winters. However, the TRB is a low-elevation and rain-fed basin, and the CRB is a high-elevation and snow-fed basin in winter (Laenen and Risley, 1997). These basins could be differently affected by climate change because snowmelt change at the CRB is more sensitive to change in both precipitation and temperature (Graves and Chang, 2007), while TRB runoff is sensitive to change in precipitation (Praskievicz and Chang, 2011; Franczyk and Chang, 2009).

We quantify and analyze the uncertainty in future streamflow by combining the uncertainty in future GHG emission scenarios, GCM structures, and the hydrologic model parameters. The following research questions are addressed and discussed: (1) What are the relative influences of uncertainty from the above sources according to streamflow responses to climate change in the two basins? And, what are the main sources of uncertainties affecting the changes in streamflow under climate change? (2) How will the relative uncertainties stemming from diverse sources vary over time in the two basins? A brief description of two study areas is presented in Section 2. A detailed description of the GCM simulations and the downscaling method, the hydrological model, and sampling scheme used in parameter uncertainty analysis is provided in Section 3. Section 4 elaborates on the results by analyzing the effects of various sources of uncertainty on projecting the changes in streamflow at the short and seasonal time scales in the two basins. A discussion and conclusion are provided in Sections 5 and 6.

2. Study area and data

The TRB (1847 km^2) and the CRB (2529 km^2), located west and east of Portland, Oregon in the USA, are major tributaries to the Willamette River (see Fig. 1). They provide essential municipal, industrial, and irrigation water, as well as habitat for fish and other wildlife, and places for recreation (Laenen and Risley, 1997; Rounds and Wood, 2001). These basins have a temperate marine climate characterized by dry summers and wet winters. Approximately 80% of precipitation in both basins falls from October to May (Chang, 2007). The inter-annual precipitation variability in this region is associated with large scale atmospheric circulation processes, such as El Niño-Southern Oscillation (ENSO) and Pacific Decadal Oscillation (PDO). Praskievicz and Chang (2009b) demonstrated that ENSO teleconnections are strongest at the beginning and end of the rainy season for winter heavy precipitation events, while the PDO dominates in midwinter.

The two basins lie at different elevations (see Fig. 1). In the low region below 1000 m, rain-fed and relatively impermeable substrates lead to flow regimes that are more responsive to seasonal patterns of precipitation (Poff, 1996). Because most areas of the TRB lie at low elevations, precipitation is in the form of rainfall except in the Coast Range Mountains on the far west. The flow regime in the high elevation region above 1000 m is strongly influenced by a combination of snow-dominated precipitation, landform, and volcanic bedrock geology (Tague and Grant, 2004; Chang and Jung, 2010). A study by Laenen and Risley (1997) showed that approximately 35% of the annual precipitation falls as snow at 1000 m elevation in this region. Young volcanic bedrock geology causes more constant or moderated flow regime through time (Graves and Chang, 2007; Tague et al., 2008). Therefore, streamflow in the CRB has less flooding in winter and greater streamflow during summer and autumn than in the TRB.

To calibrate the hydrologic model parameters, we collected hydroclimatologic and topographic data. Daily maximum and minimum temperature and precipitation data were obtained from the National Oceanic and Atmospheric Administration Cooperative Observer Program (NOAA COOP, 2009) for 1972–2007. Fig. 1 shows the weather stations used in this study. These stations were selected based on the completeness of their records, with less than 5% missing data. The missing values of precipitation and temperature were interpolated by using the monthly regression method based on contiguity. Two streamflow gauging station data were also used to evaluate the performance of the hydrologic model (USGS NWIS, 2011). Snow water equivalent data from the Natural Resources Conservation Service Snow Telemetry (NRCS SNOTEL, 2011) were used to verify the accuracy of snowmelt simulation of the hydrologic model. We chose the Peavine Ridge station which has an elevation of 1042 m and a data record starting in 1985. Additionally, soil maps (NRCS, 1986), land cover (Fegeas et al., 1983), geology data (McFarland, 1983) and topographic data based on a Digital Elevation Model (DEM) (USGS, 1990) were also used for modeling purposes.

3. Methodology

3.1. Climate change simulations used in this study

We used 16 (8 GCMs with 2 GHG emission scenarios) downscaled climate data scenarios provided by the Climate Impacts

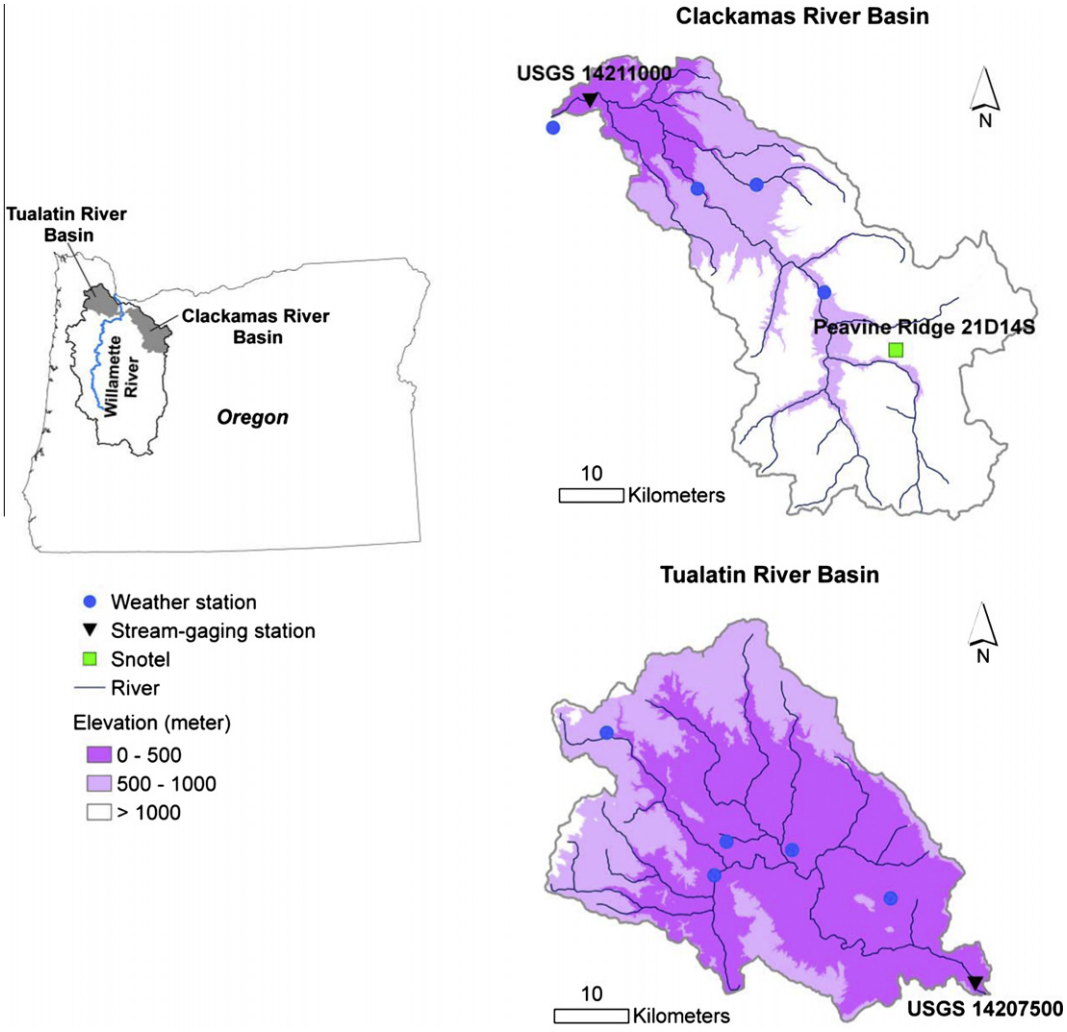

Fig. 1. Clackamas River Basin and Tualatin River Basin.

Table 1
Description of Global Climate Models used in this study (Randall et al., 2007).

Model ID	Abbreviation	Country	Resolution		Reference
			Atmosphere	Ocean	
CCSM3	CCS	USA	1.4° × 1.4°	1.0° × 1.0°	Collins et al. (2006)
CNRM-CM3	CNR	France	1.9° × 1.9°	2.0° × 2.0°	Terray et al. (1998)
ECHAM5/MPI-OM	EH5	Germany	1.9° × 1.9°	1.5° × 1.5°	Jungclaus et al. (2006)
ECHO-G	ECH	Germany/Korea	3.9° × 3.9°	2.8° × 2.8°	Min et al. (2005)
IPSL-CM4	IPS	France	2.5° × 3.75°	2.0° × 2.0°	Marti et al. (2005)
MIROC3.2(hires)	MIR	Japan	1.1° × 1.1°	0.2° × 0.3°	K-1 Developers (2004)
PCM	PCM	USA	2.8° × 2.8°	0.7° × 1.1°	Washington et al. (2000)
UKMO-HadCM3	HAD	UK	2.5° × 3.75°	1.25° × 1.25°	Gordon et al. (2000)

Group (CIG) at the University of Washington for integrated assessment of climate change impacts in the Pacific Northwest (see Table 1). They selected the GCM simulations from the IPCC Fourth Assessment Report (IPCC, 2007) based on their skill at simulating the 20th century in the Pacific Northwest (Salathé et al., 2007). To assess the uncertainty due to emission scenarios, the Special Report on Emission Scenarios (SRES) (IPCC, 2000) A1B and B1 scenarios were selected. Many researchers have used these scenarios because they present a slightly high GHG emission condition (CO_2 concentration is up to 720 ppm in year 2100) and a low condition (CO_2 concentration is up to 550 ppm in year 2100), respectively. The SRES A1B and B1 emission scenarios are similar in total radiative forcing until the mid-century (up to 2050), but later in the century, the A1B produces considerably more radiative forcing than the B1 emission scenario.

Although GCMs are useful for comprehensive projections of future climate condition, they yield relatively coarse spatial resolution results of approximately 150–300 km so that they are unable to resolve significant sub-grid scale features such as topography, clouds, and land use (e.g., Im et al., 2010). To account for these sub-grid processes, many studies have employed various downscaling methods (e.g. Wood et al., 2004; Najafi et al., 2011a;

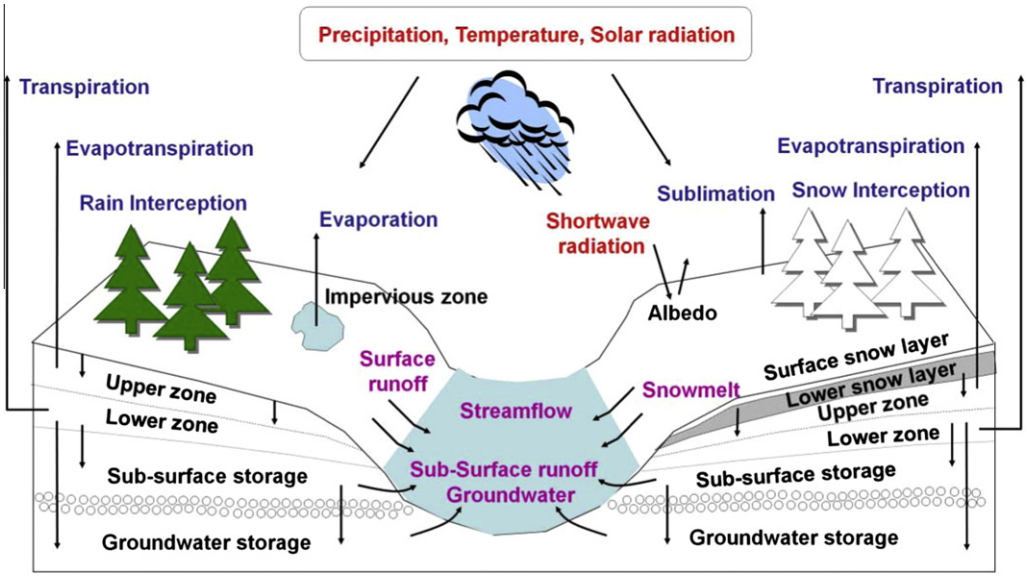

Fig. 2. Precipitation Runoff Modeling System (PRMS) schematic.

Halmstad et al., 2012). Through downscaling, it is possible to represent the sub-grid scale spatial climate patterns for regional hydrologic impact assessment under climate change. The CIG used statistical downscaling, the so-called bias correction and spatial downscaling (BCSD) method based on quantile mapping (Wood et al., 2002; Salathé, 2005). They disaggregated the monthly GCM simulation to daily data at the spatial resolution of 0.0625 degree (approximately 5–7 km). This method has three steps. The first step is the spatial downscaling of the climate variables from a GCM scale grid to a regional scale grid, depending on the scale factor calculated from monthly gridded observed data. The next step is bias correction for spatially downscaled data using the historic station data based on the transfer function between spatially downscaled GCM simulation and observed data. Finally, the monthly precipitation and maximum and minimum temperature data are disaggregated to daily time series using the historic daily data, modified by the perturbation factor of the future period. However, this downscaling method has a couple of limitations. First, it cannot resolve the sequencing of extreme events because of using monthly GCM simulations. Second, the accuracy of this method could vary based on density and quality of historical climatologic stations that are used to develop the gridded monthly observed data (Salathé, 2005). Also it should be noted that the performance of any regression based statistical downscaling method is heavily dependent upon the predictors used in the procedure. Najafi et al. (2011b) explained the importance of an objective procedure to select the most relevant predictors in a statistical downscaling method and used an optimal predictor selection procedure, developed by Moradkhani and Meier (2010), in statistical downscaling of precipitation over a basin in the Pacific Northwest of US.

3.2. Precipitation Runoff Modeling System (PRMS)

PRMS was developed to analyze the effect of climate and land use changes on water resources (Leavesley et al., 1983). It has been applied in several regional assessment studies to investigate the impact of climate change on water resources in a variety of climatic and physiographic regions (e.g. Burlando and Rosso, 2002; Dagnachew et al., 2003; Bae et al., 2008a; Im et al., 2010; Jung and Chang, 2011). To better understand the wide array of individual and combined factors that can affect the hydrologic response in a watershed system, Risley et al. (2011) employed PRMS, driven by GCM outputs, in 14 watersheds across the US, and conducted a comparative statistical analysis on the outputs. PRMS has been successfully used in simulating flow in snow-dominated basins (e.g. Leavesley et al., 2002; Dressler et al., 2006).

PRMS is a physically-based hydrologic model that uses distributed-parameters based on Hydrologic Response Units (HRUs) (Leavesley and Stannard, 1995) (see Fig. 2). Each HRU is assumed to be homogeneous with respect to its hydrologic response to precipitation and temperature. HRUs are partitioned based on topographic attributes, such as elevation, slope, aspect, land use, soil type, and geology. Each HRU is conceptualized as an interconnected series of reservoirs – interception, snow zone, two soil zone, subsurface reservoir, and groundwater reservoir – whose combined output produces the total hydrologic response. In this study HRUs were delineated by reclassifying slope and aspect into six groups, land use into six groups, geology into five groups, and soil data into four groups. In total, 208 and 262 HRUs were created for the CRB and TRB, respectively.

To calculate the spatially distributed precipitation for each HRU based on observed climate station data, we employed the Precipitation elevation Regressions on Independent Slopes Model (PRISM) data (OCS, 2011). PRISM, a high quality gridded climate data set with 800 m resolution, provides average monthly precipitation, maximum and minimum temperature data for 1971–2000. Monthly spatial factors for each PRISM gird point were obtained by comparing monthly mean precipitation value of weather station and the contiguous PRISM grids. For HRUs, the monthly spatial factors were estimated by using the area weighted method, and then these factors were multiplied by the observed precipitation. The monthly maximum and minimum temperature for HRUs are obtained based on a lapse rate according to elevation (Laenen and Risley, 1997).

PRMS successively simulates a water balance for each day and an energy balance for each 12 h, depending on daily precipitation and maximum and minimum temperatures as model inputs (Hay et al., 2009). The water balance computation includes evapotranspiration, interception, snowmelt, soil moisture accounting, surface runoff, subsurface runoff, and groundwater runoff (see Fig. 2). Energy balance equations control snowpack accumulation and snowmelt processes. The parameters related to topographic variables,

Table 2
Description of PRMS model parameters for optimization.

Parameter	Description	Range	Default
adjmix_rain	Adjustment factor of rain proportion in mixed rain/snow event	0.0–3.0	1.0
cecn_coef	Convection condensation energy coefficient	0.0–20.0	5.0
emis_noppt	Emissivity of air on days without precipitation	0.757–1.000	0.757
freeh2o_cap	Free-water holding capacity of snowpack	0.01–0.20	0.05
gwflow_coef	Ground-water routing coefficient	0.000–1.000	0.015
smidx_coef	Coefficient in nonlinear surface runoff contributing area algorithm	0.0001–1.0000	0.01
smidx_exp	Exponent in nonlinear surface runoff contribution area algorithm	0.2–0.8	0.3
soil2gw_max	Maximum rate of soil water excess moving to ground water	0.0–5.0	0.0
ssrcoef_sq	Coefficient to route subsurface storage to streamflow	0.0–1.0	0.1
ssrcoef_lin	Coefficient to route subsurface storage to streamflow	0.0–1.0	0.1
ssr2gw_exp	Coefficient to route water from subsurface to groundwater	0.0–3.0	1.0
ssr2gw_rate	Coefficient to route water from subsurface to groundwater	0.0–1.0	0.1
tmax_allsnow	Precipitation assumed snow if HRU maximum temperature is below this value (°C)	−23.3 to 4.4	0.0
tmax_allrain	Precipitation assumed rain if HRU maximum temperature is above this value (°C)	−17.8 to 32.2	4.4

Table 3
Change in annual precipitation and temperature in future 20-year time-slice periods relative to 1960–1989 reference period.

Period	Clackamas River Basin				Tualatin River Basin			
	Precipitation		Temperature		Precipitation		Temperature	
	A1B	B1	A1B	B1	A1B	B1	A1B	B1
2010s (2000–2019)	−2 (−6 to 6)	−1 (−9 to 5)	1 (1–2)	1 (1–2)	−2 (−8 to 7)	−1 (−9 to 6)	1 (1–2)	1 (1–2)
2020s (2010–2029)	−1 (−7 to 4)	0 (−8 to 10)	2 (1–3)	2 (1–3)	0 (−7 to 4)	0 (−8 to 10)	2 (1–2)	2 (1–2)
2030s (2020–2039)	0 (−3 to 4)	1 (−5 to 7)	3 (2–3)	2 (1–3)	1 (−3 to 6)	1 (−6 to 8)	2 (2–3)	2 (1–3)
2040s (2030–2049)	2 (−6 to 7)	0 (−6 to 6)	3 (2–4)	3 (1–3)	3 (−6 to 9)	1 (−7 to 6)	3 (2–4)	3 (2–3)
2050s (2040–2059)	3 (−3 to 10)	−1 (−8 to 15)	4 (3–5)	3 (2–4)	4 (−1 to 12)	−1 (−9 to 16)	4 (2–5)	3 (2–4)
2060s (2050–2069)	2 (−7 to 14)	0 (−11 to 15)	5 (3–6)	3 (2–4)	2 (−6 to 17)	1 (−10 to 16)	4 (3–5)	3 (2–4)
2070s (2060–2079)	2 (−7 to 13)	0 (−12 to 9)	5 (4–6)	4 (2 to 5)	2 (−6 to 16)	1 (−12 to 10)	5 (4–6)	4 (2–5)
2080s (2070–2089)	3 (−6 to 12)	1 (−6 to 7)	6 (5–7)	4 (3–5)	4 (−7 to 14)	1 (−5 to 7)	5 (4–7)	4 (3–5)
2090s (2080–2099)	5 (−5 to 17)	3 (−5 to 13)	6 (5–8)	5 (3–6)	6 (−7 to 20)	4 (−5 to 14)	6 (4–87)	4 (3–6)

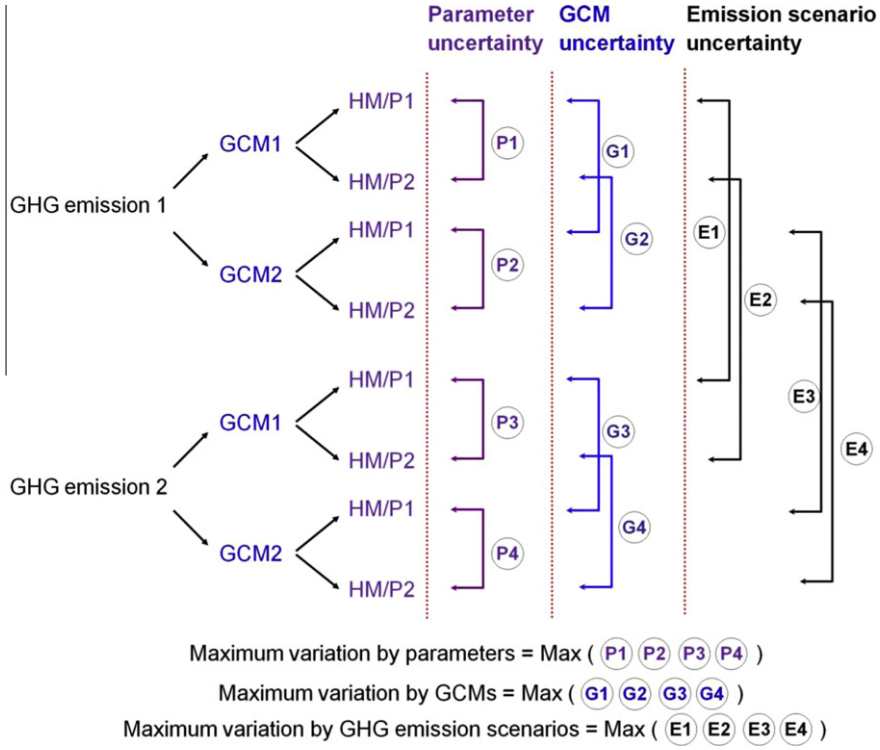

Fig. 3. Concept of estimation of maximum variation derived by each uncertainty sources such as hydrological model parameter sets, GCMs, and GHG emission scenarios.

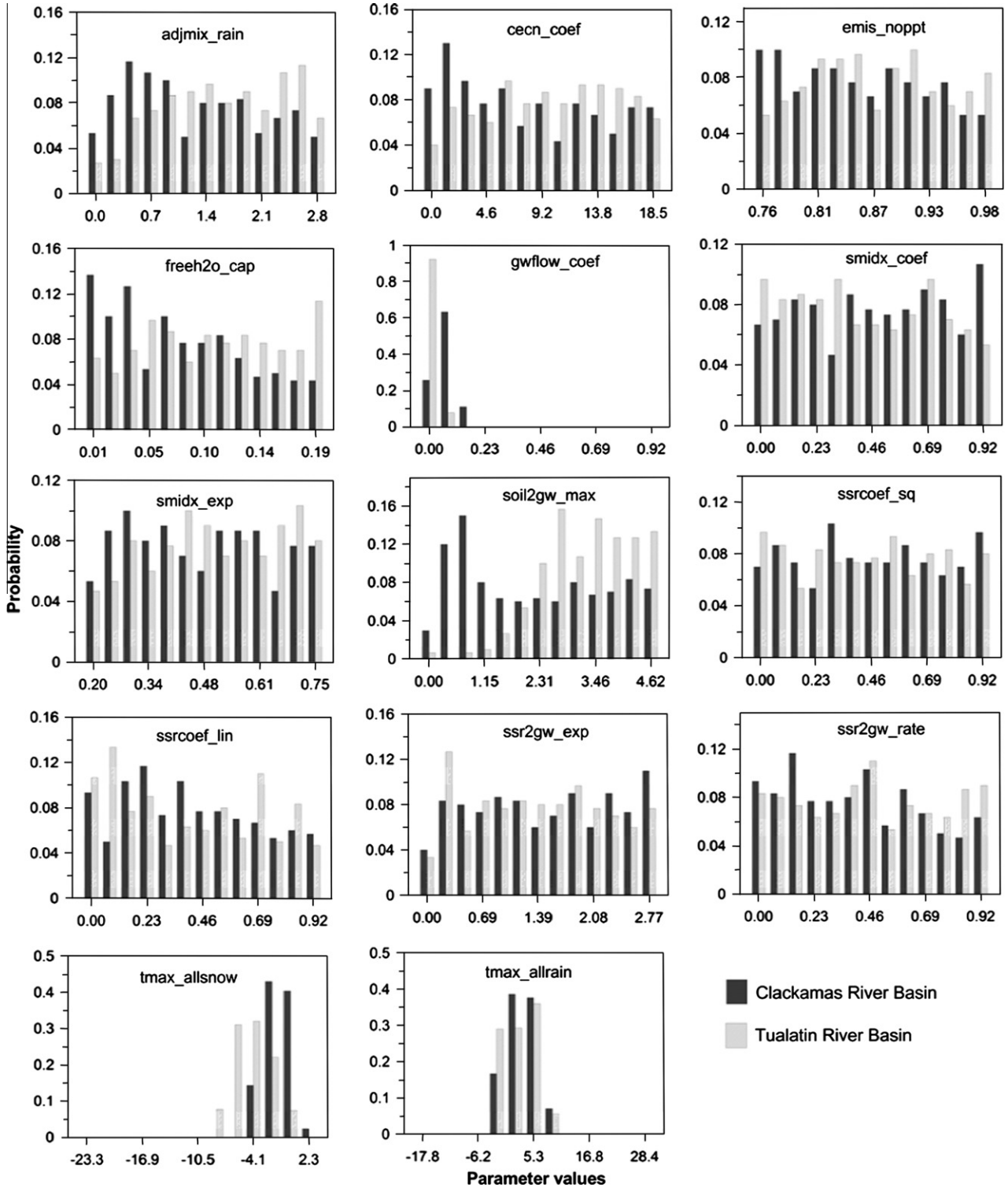

Fig. 4. Distribution of estimated parameters of PRMS model.

such as area, slope, elevation, soil type and soil moisture capacity, ratio of impervious area, and seasonal vegetation cover density according to land cover are directly estimated from the measurable basin characteristics using GIS (Hay and Clark, 2003; Bae et al., 2008b; Im et al., 2010). However, the other parameters determining the timing and amount of runoff need to be calibrated (see Table 2). There are 20 parameters related to snow modeling in PRMS. This study used the values recommended by Leavesley et al. (1983) except *tmax_allsnow*.

The type of precipitation (i.e., rain or snow) can be determined by two parameters, *tmax_allsnow* and *tmax_allrain* as the thresholds of the maximum temperature. If maximum temperature of each HRU is above the *tmax_allsnow* and below the *tmax_allrain*, precipitation is assumed to be mixed with snow and adjusted by

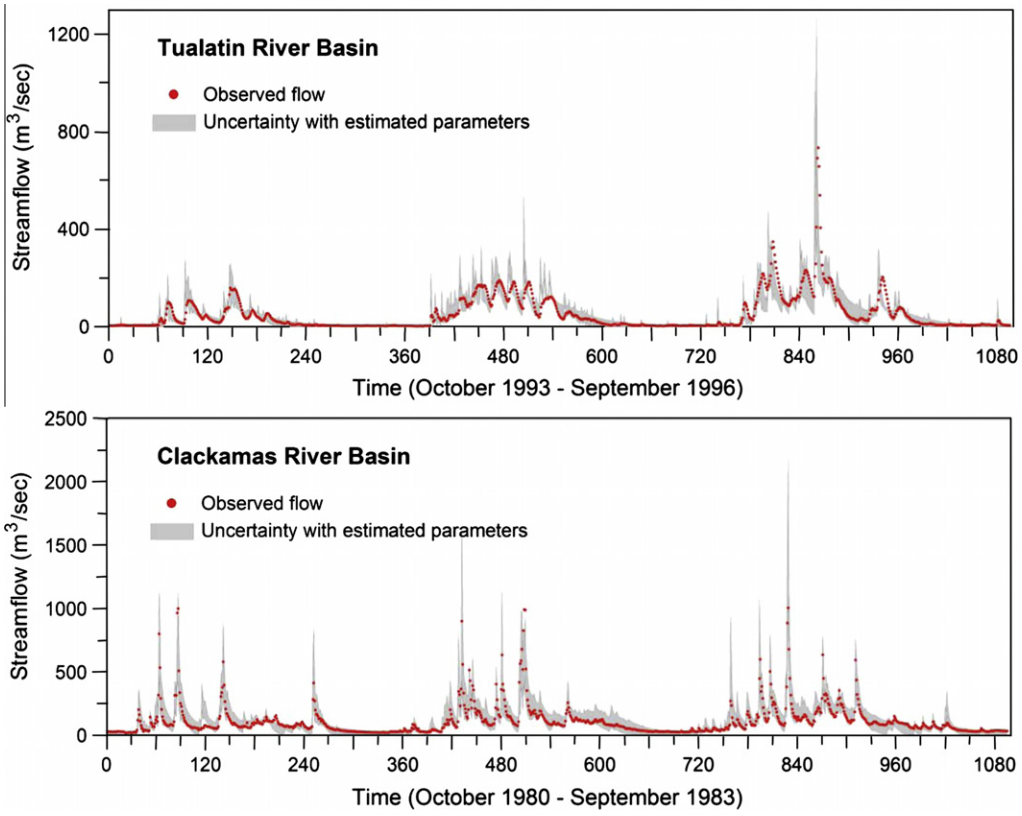

Fig. 5. Observed streamflow (filled circle) and ranges of simulated streamflow with estimated parameters.

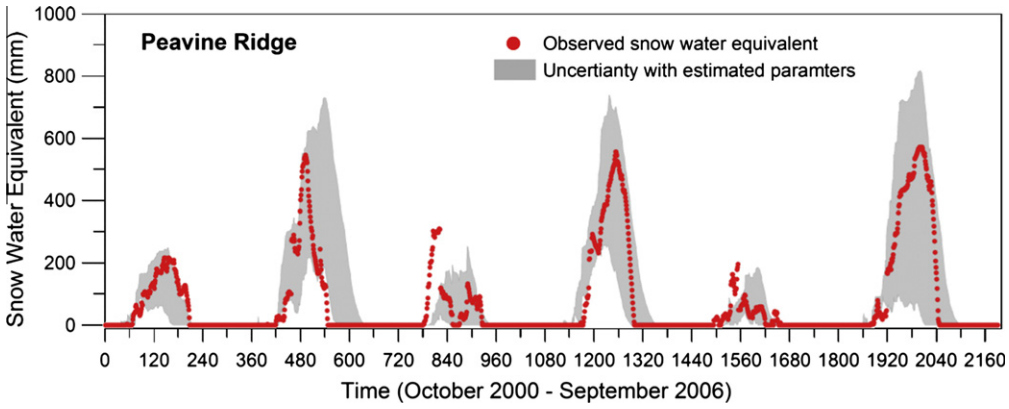

Fig. 6. Performance of simulations of snow water equivalent using estimated parameters at the Peavine Ridge (21D14S) SNOTEL sites in Clackamas River Basin.

adjmix_rain. The snow process in the PRMS model includes initiation, accumulation, and depletion of a snowpack as described by Obled and Rosse (1977). Snowmelt occurs when the temperature of snowpack, calculated by energy balance (*cecn_coef*, *emis_noppt*), reaches isothermal conditions at 0 °C. Snowmelt is first used to satisfy the freewater holding capacity of the snowpack (*freeh2o_cap*) and then becomes infiltration or surface runoff. The surface runoff is computed using a nonlinear equation (*smidx_coef*, *smidx_exp*), depending on antecedent soil moisture and rainfall amount. Infiltrated soil water first satisfies the groundwater reservoir based on a recharge rate (*soil2gw_max*). When the percolating moisture exceeds the *soil2gw_max*, the excess soil water goes to the subsurface reservoir. Excess moisture in the subsurface reservoir either percolates to a ground-water reservoir (*ssr2gw_exp*, *ssr2gw_rate*) or flows to stream (*ssrcoef_sq*, *ssrcoef_lin*). Groundwater is simulated conceptually by a linear reservoir characterized by parameter *gwflow_coef*. More detailed description of model conceptualization and the governing equations is provided in Leavesley et al. (1983) and Leavesley and Stannard (1995).

For potential evapotranspiration calculation, the Hamon method was used (Hamon, 1961) because it is simple and the needed temperature data were readily available. This method is well-suited to a large range of surface types with comparatively little bias (e.g. Federer et al., 1996; Vörösmarty et al., 1998; Kleinen and

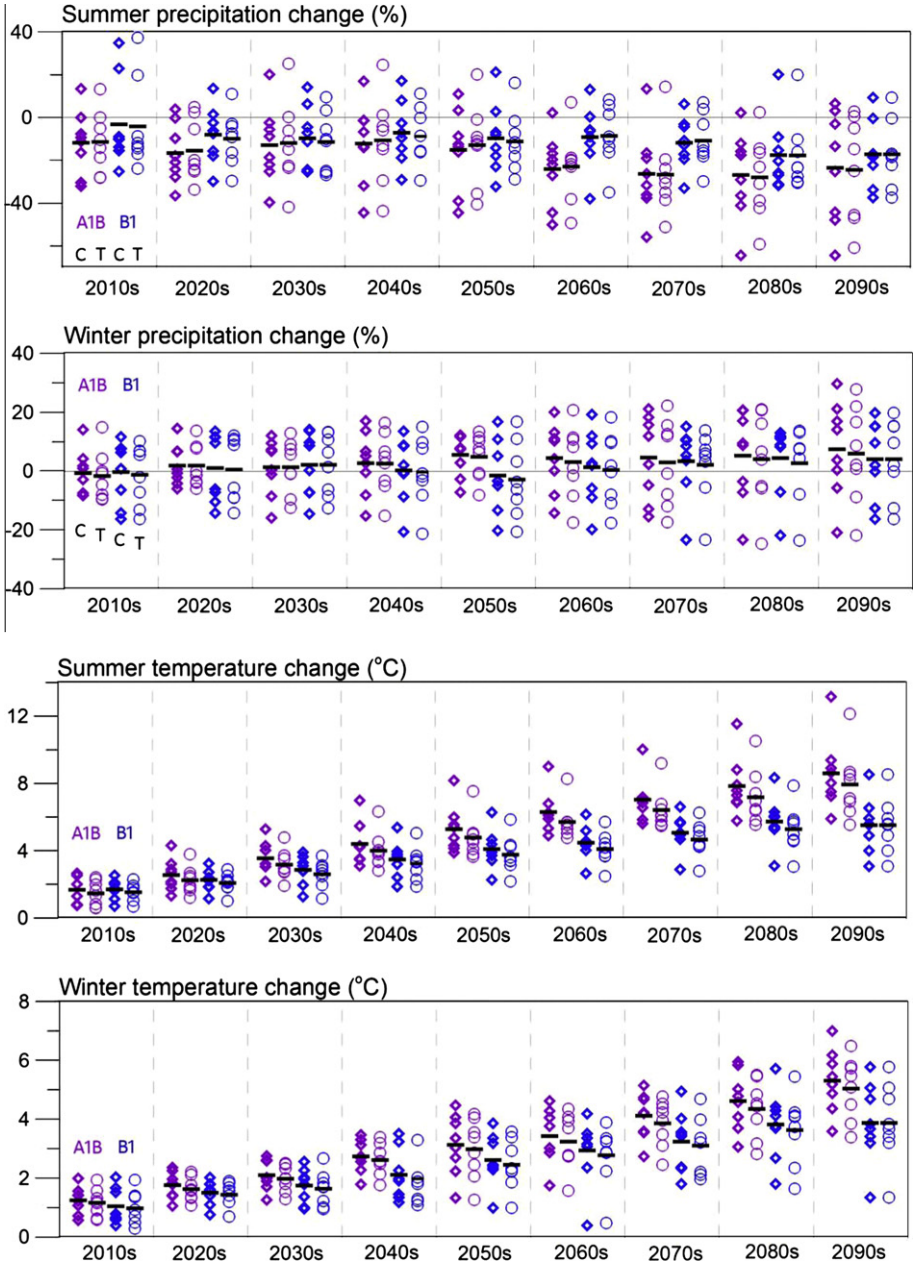

Fig. 7. Change in summer and winter precipitation (two upper panels) and temperature (two lower panels) in future period relative to the reference period 1960–1989. Symbols indicate each GCM simulation for CRB (C, diamond) and TRB (T, circle). Purple and blue colors represent A1B and B1 GHG emission scenarios respectively. Black horizontal bar represents mean value. (For interpretation of the references to color in this figure legend, the reader is referred to the web version of this article.)

Petschel-Held, 2007). However, Shaw and Riha (2011) argued the temperature-based PET method such as the Hamon method could exaggerate PET in a warming climate.

3.3. Assessment of uncertainty

To evaluate the effects of uncertainty from a variety of sources in the two basins, eight GCM simulations driven by two emission scenarios (A1B and B1) for the full period 1960–2099 were fed to the PRMS model as inputs. The seasonal mean values in climate and runoff were calculated based on the transient series for nine standard time-slices (see Table 3) and compared with the reference period of 1960–1989. To address the model parameter uncertainty, 14 PRMS parameters (see Table 2) were carefully selected as suggested in the literature (e.g. Hay et al., 2006, 2009; Bae et al., 2008b; Im et al., 2010). These studies demonstrated that PRMS could closely reproduce observed flows when sensitive parameters were calibrated.

This study examined the relative influences of uncertainty sources on seasonal (winter: December, January, and February and summer: June, July, and August) and extreme (10th (Q10) and 90th (Q90) percentile) runoff changes by comparing the maximum variations according to each uncertainty source (see Fig. 3). For instance, if we had employed only two GCMs, two GHG emission scenarios, and two hydrologic parameter sets for the climate change impact analysis as shown in Fig. 3, eight combinations would have been generated. Using such combinations we first calculated differences between the two results that are derived from different hydrologic parameter sets where other forcing conditions are identical. Finally, we determined the lowest and highest runoff

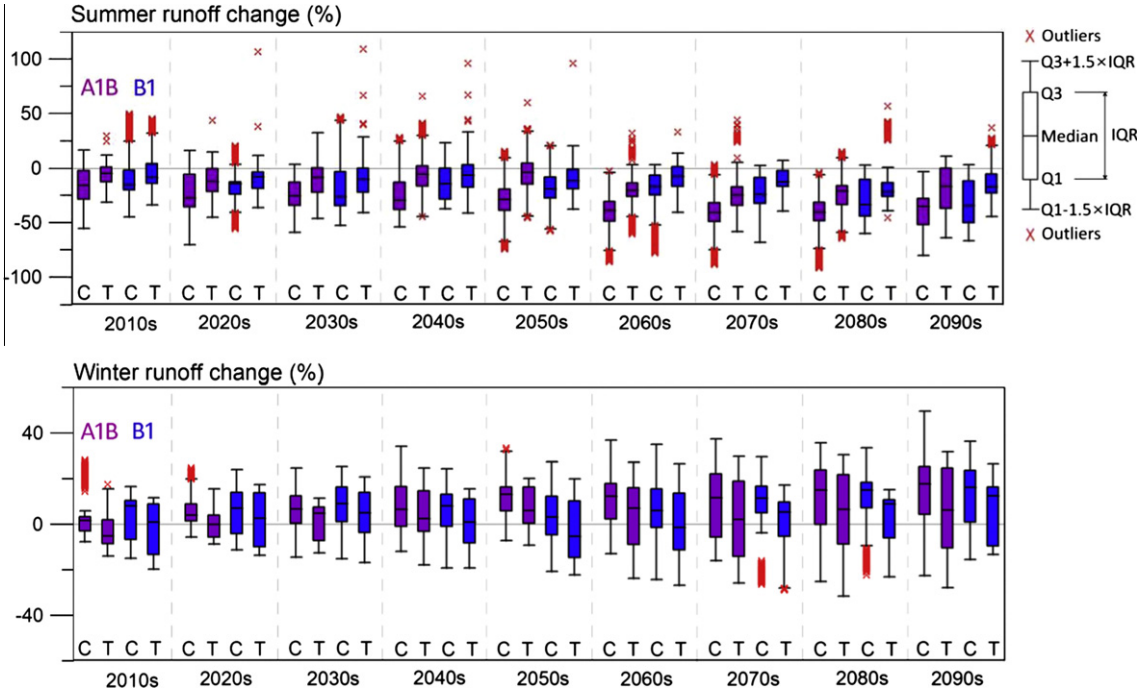

Fig. 8. Change in summer and winter runoff of CRB (C) and TRB (T) in future period relative to 1960–1989 reference period. Purple and blue colors represent A1B and B1 GHG emission scenarios respectively. Box and whisker plot shows median value (bar) in the box, Q1 is 25th percentile value, Q3 is 75th percentile value, Q3–Q1 is interquartile range (IQR), upper whisker is the highest datum within 1.5 × IQR of the higher quartile, lower whisker is the lowest datum within 1.5 × IQR of the lower quartile. Outliers are symbols shown by "x". (For interpretation of the references to color in this figure legend, the reader is referred to the web version of this article.)

changes that give the greatest difference between them. The same procedure was applied to determine the greatest difference associated with the other uncertainty sources.

3.4. Latin Hypercube Sampling (LHS) of the model parameters

The Monte Carlo methods are often used to explore the parameter space of hydrologic models to obtain the behavioral parameter sets. To initialize such a process, and to uniformly generate the parameter sets from feasible ranges (see Table 2 for parameter ranges), the LHS method (McKay et al., 1979) can be used.

LHS was developed to generate well-distributed plausible collections of parameter sets in multi-dimensional space (Iman et al., 1981). LHS is commonly used to reduce the number of runs necessary for a Monte Carlo approach to achieve a reasonably accurate random distribution (Davey, 2008). Davey (2008) compared the representation capacity of LHS and Monte Carlo approach for one- and two-variable function in the magnetic field optimization. The results showed that the samples from LHS closely represented the actual function. This indicates that LHS effectively reduces the number of simulations necessary to sufficiently sample a population of multiple variables. To generate the PRMS parameter sets used in this study, LHS was undertaken with 20,000 runs.

3.5. Obtaining and testing PRMS parameter sets

Randomly generated parameter sets from plausible ranges (Table 2) were used to simulate daily runoff using observed daily precipitation and maximum and minimum temperature for the period of 1973–1983 in the CRB and the period of 1973–2006 in the TRB. The first 2 years of the PRMS simulations are used for model spin-up and were not considered for further analysis. The Nash–Sutcliffe (1970) non-dimensional model efficiency criterion, NS, defined by Eq. (1), was used as the objective function.

$$\mathrm{NS} = 1 - \frac{\sum_{i=1}^{n}(O_i - S_i)^2}{\sum_{i=1}^{n}(O_i - \overline{O}_i)^2} \quad (1)$$

where O_i and S_i are respectively the ith observed and simulated streamflow, and $\overline{O}_i$ is the observed mean streamflow.

In this study we assumed that a NS value above 0.7 indicates a satisfactory fit between observed and simulated hydrographs (see Freer et al., 1996; Wilby, 2005; Choi and Beven, 2007). A total of 389 parameter sets for the CRB and 926 parameter sets for the TRB were obtained as behavioral parameters. To compare the differing parameter uncertainties of the two basins, 300 best-performing parameter sets with the highest NS values were chosen for each basin. Fig. 4 shows distributions of the selected 300 parameter sets in the two basins. Although the distributions of most of the parameters are similar, significant differences in distributional properties of *soil2gw_max* and *tmax_allsnow* parameters are seen in the two basins. *soil2gw_max* parameter for the TRB tends toward higher values but the parameter values of the CRB show a relatively uniform distribution. For *tmax_allsnow* parameter, the lower uncertainty is seen in the CRB as compared with the TRB. Fig. 5 displays daily observed flow and range of simulated flow using the selected parameters. This range well covers observed low and high flows indicating that PRMS with the selected parameters would reasonably simulate the observed streamflow. The observed SWE from Peavine Ridge SNOTEL station plotted against simulated SWE using the selected 300 behavioral parameters sets for CRB (see Fig. 6). The NS for SWE estimation ranges from 0.47 to 0.72 between observed and simulated values.

4. Results

4.1. Changes in seasonal precipitation and temperature

Fig. 7 shows the changes in seasonal precipitation and temperature for the nine time-slices relative to the reference period of

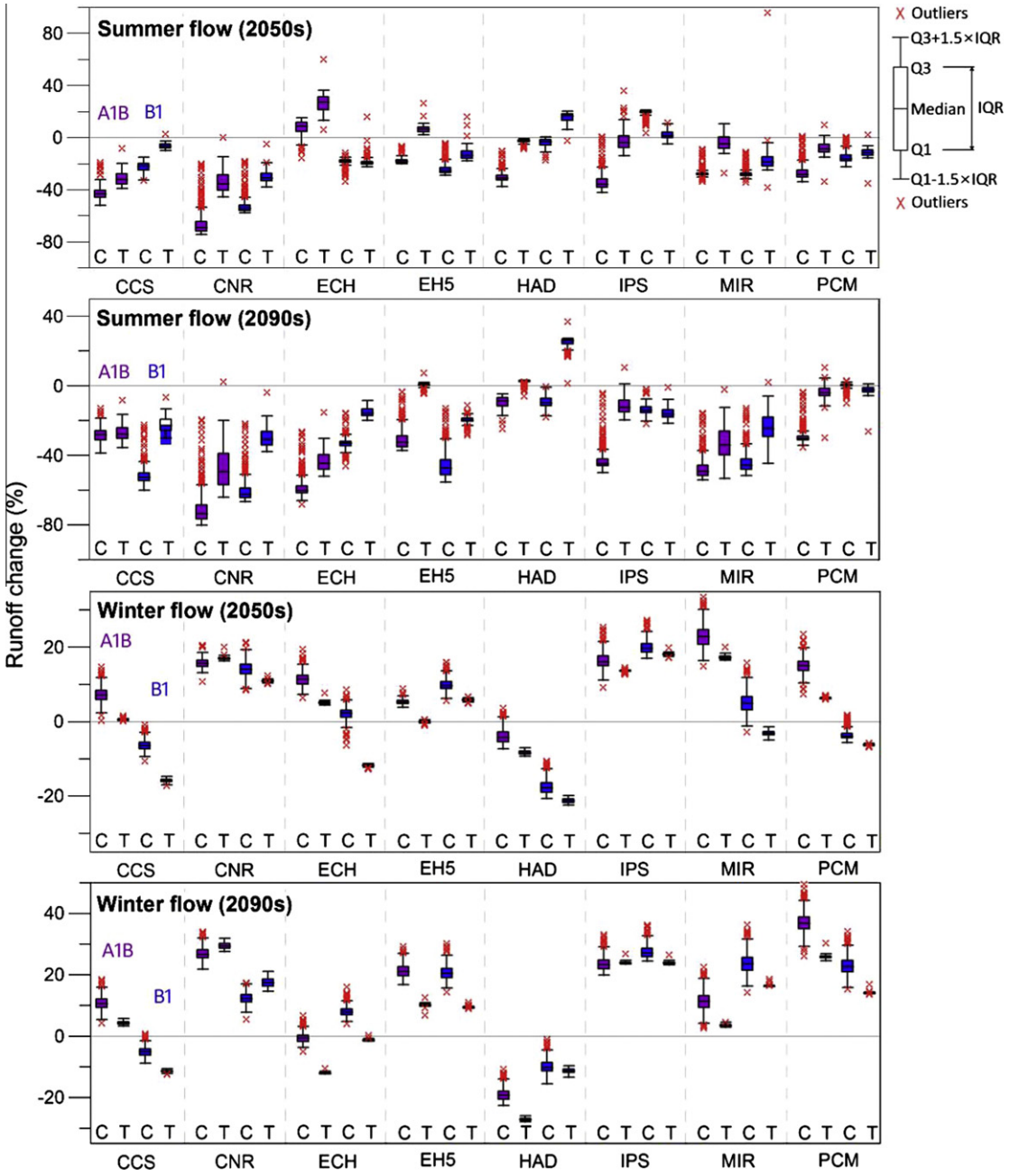

Fig. 9. Change in summer and winter runoff of CRB (C) and TRB (T) for 2050s and 2090s based on each eight GCMs and two emission scenarios. Purple and blue colors represent A1B and B1 GHG emission scenarios respectively. Box and whisker plot shows median value (bar) in the box, Q1 is 25th percentile value, Q3 is 75th percentile value, Q3–Q1 is interquartile range (IQR), upper whisker is the highest datum within 1.5 × IQR of the higher quartile, lower whisker is the lowest datum within 1.5 × IQR of the lower quartile. Outliers are symbols shown by "x". (For interpretation of the references to color in this figure legend, the reader is referred to the web version of this article.)

1960–1989. This figure shows that the precipitation and temperature changes according to GCMs and GHG emission scenarios for the two basins differ by the time-slices as well as the summer and winter seasons. However, no substantial differences in precipitation and temperature changes are seen between the two basins. As shown in this figure, the ranges of seasonal climate changes by GCMs are relatively larger than those of the GHG emission scenarios in both basins. Similar findings have been reported in other studies (e.g., Wilby and Harris, 2006; Bates et al., 2008; Kay et al., 2009; Prudhomme and Davies, 2008; Chang and Jung, 2010; Bae et al., 2011). Fig. 7 also shows that the seasonal changes of precipitation and temperature are higher in summer than in winter season. The ranges of changes in temperature increases with time, but the changes in precipitation do not reveal a considerable trend. Table 3 shows ensemble mean and ranges for change in annual precipitation and temperature for the nine time-slices relative to the reference period. Although the change in annual precipitation is low compared to that in seasonal precipitation, it shows that the uncertainty ranges from GCMs are relatively larger than those of GHG emission scenarios or basins.

4.2. Uncertainty of seasonal runoff change

Fig. 8 displays the box–whisker plot of the changes in the summer and winter runoff. The uncertainty ranges of summer runoff

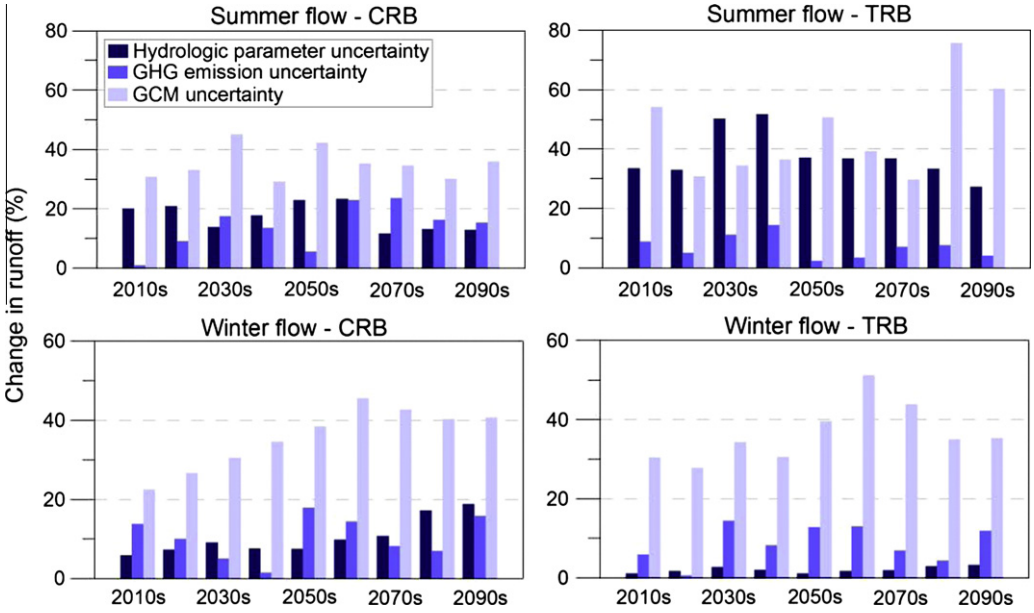

Fig. 10. Maximum range of change in summer and winter runoff according to hydrologic parameters, GHG emission scenarios, and GCMs.

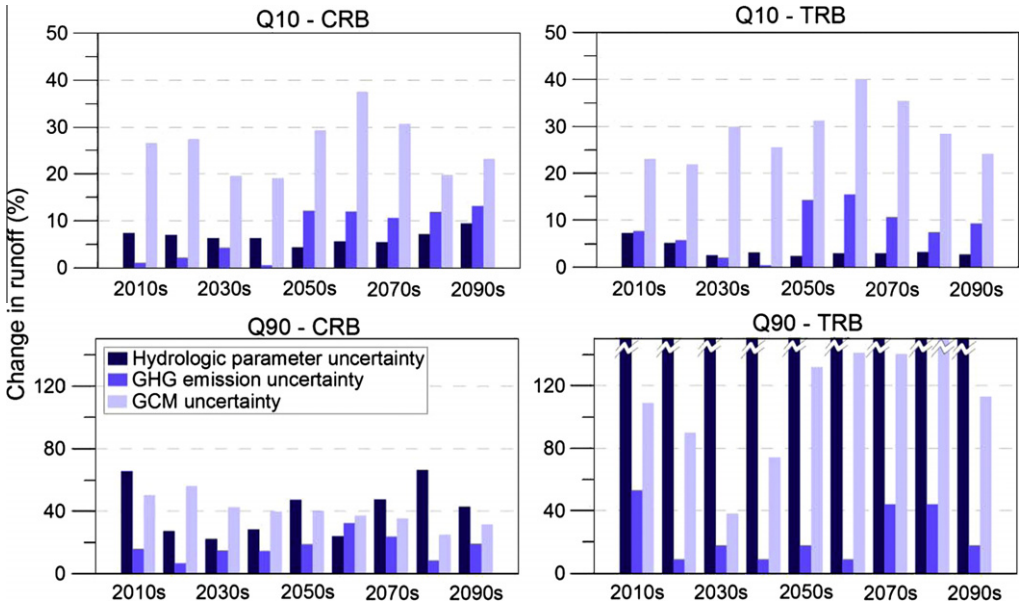

Fig. 11. Maximum range of change in high flow (Q10) and low flow (Q90) according to hydrologic parameters, GHG emission scenarios, and GCMs.

change are relatively larger than those in winter. This could be attributed to the seasonal variation of runoff in this region. Knowing that the summer is the driest season, a small change in the amount of precipitation would result in a substantial relative change in summer runoff. Wilby et al. (2006) showed that UK basins have similar seasonal variation in runoff uncertainty; summer flows are projected to decline with high uncertainty, while annual flows are projected to increase only slightly. Im et al. (2010) had similar findings in a Korean basin, although with contrasting seasonal variation of runoff, as dry winter and wet summer where the uncertainty in change in the absolute amount of runoff is larger in winter than summer.

The seasonal runoff changes of both basins show that the uncertainty stemming from GCMs is greater than that due to GHG emission scenarios. The predictive uncertainty range varies over time, particularly for summer runoff changes, however, the uncertainty range of winter runoff changes for the second half of the 21st century (after the 2050s) is wider than those in the first half of the 21st century (before the 2050s) (see Fig. 8). Hawkins and Sutton (2009) explained that the uncertainty in regional climate predictions varies with time and across spatial and temporal scales. Our study also confirms that the uncertainty in runoff change varies spatially and temporally.

Fig. 9 displays seasonal runoff change for the two periods of 2050s and 2090s with respect to uncertainty sources including eight GCMs, two emission scenarios, and 300 hydrologic parameters. An interesting result is that the winter runoff changes due to the hydrologic parameters exhibit a remarkably different range

between the two basins. The range of winter runoff change in the TRB is much smaller than in the CRB. This result indicates that winter runoff change in the rain-dominated TRB is less affected by hydrologic parameters uncertainty. However, the uncertainty ranges in summer runoff change are similar in the two basins, except for CNR, EH5, and MIR in 2090s.

Fig. 10 shows the relative contribution of uncertainty from various sources, which is estimated by the method described in Section 3.3. To obtain the maximum range of hydrologic parameter uncertainty, we found the lowest and highest runoff changes over the 300 parameter sets under the same GCM and the same emission scenario. Of the 16 lowest/highest pairs (8 GCMs × 2 emission scenarios), we picked the pair with the greatest difference between them, and plotted it in Fig. 10. For GHG emission scenario uncertainty, we obtained the lowest and highest runoff changes over the two emission scenarios among 2400 pairs (8 GCMs × 300 parameter set). Also, GCM uncertainty was calculated through the same process except using 600 pairs (2 emission scenarios × 300 parameter sets). The analysis of uncertainty in the winter runoff suggests that the GCM uncertainty is the highest, however, the relative contribution of emission scenario and hydrologic parameter uncertainties vary in the time-slices. It appears that the parameter uncertainty in the CRB is larger than that of the emission scenarios for the 2030s, 2040s, 2070s, 2080s, and 2090s while the parameter uncertainty in the TRB is lower than the emission scenario uncertainty, except 2020s. The analysis of maximum uncertainty of summer runoff change, however, shows more complex behavior. In general, relative change in summer runoff as a result of uncertainty in hydrologic parameters is considerably higher than the corresponding change in winter runoff. In some cases (e.g., 2020s, 2030s, 2040s, and 2070s) in the TRB, the uncertainty associated with hydrologic parameters is the highest. This result can be explained to the small volume of summer runoff in this region; Wilby et al. (2006) and Bae et al. (2011) noted that more caution is needed for interpreting change in future low flow condition in the climate impact study.

4.3. Uncertainty of extreme flow change

Maximum changes in low and high flows for future time-slices were examined in Fig. 11. The ensemble mean of change in the Q10 high flow slightly increases in the range of +5% to +10% in both basins, while those changes in the Q90 low flow are in the range of −60% to −10% (not shown). The change in the Q10high flow is mainly affected by the GCM uncertainty rather than GHG emission scenarios and hydrologic parameter uncertainties in both basins, although hydrologic uncertainty in the CRB appears to be larger than that of the TRB. Hence, the Q10 uncertainty of GHG emission scenarios notably increases after the 2050s. This could be attributed to A1B and B1 emission scenarios showing similar levels of GHG emissions up to 2050s but different levels toward the end of 21st century. The change in 90 low flow (Q90) at the TRB reveals substantial variation associated with hydrologic parameter uncertainty. This could be associated with the fact that the TRB's streamflow volume is lower than the CRB's during the dry season. The 90% low flow mainly occurs in summer season. Therefore, the large variation can be explained by the difference between low summer and high winter flow volumes. As shown in Fig. 11, hydrologic parameter uncertainty has higher impact on the change in low flow (Q90) than on the change in high flow (Q10).

5. Discussion

5.1. Uncertainties in seasonal and extreme flow projections

The detailed analyses of this study focus on the uncertainty in the impact of climate change on seasonal mean and extreme flows for two distinct basins. It is demonstrated that hydrological uncertainty varies significantly between the two basins given their climate regimes. The changes in runoff over different time-slices are highly variable by season and basin as a result of uncertainty in GCM, emission scenario, and hydrologic model parameter identification. Most notably, change in winter runoff in the

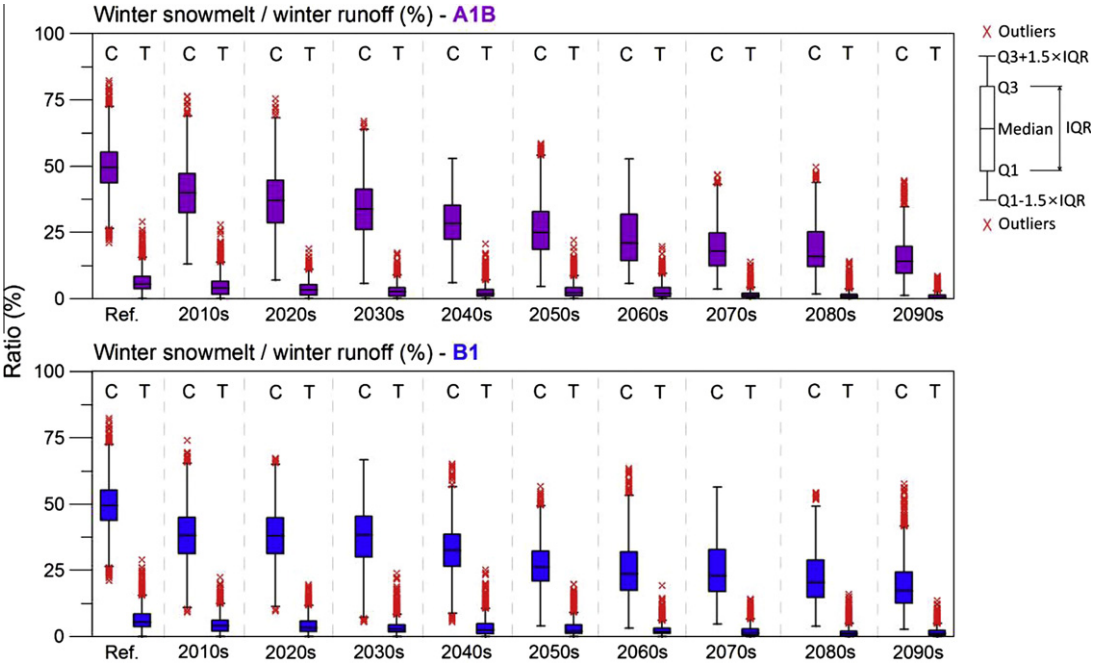

Fig. 12. Ratio of winter snowmelt to winter runoff (S/R) of CRB (C) and TRB (T) for reference period and future 9 periods. Box and whisker plot shows median value (bar) in the box, Q1 is 25th percentile value, Q3 is 75th percentile value, Q3–Q1 is interquartile range (IQR), upper whisker is the highest datum within 1.5 × IQR of the higher quartile, lower whisker is the lowest datum within 1.5 × IQR of the lower quartile. Outliers are symbols shown by "x".

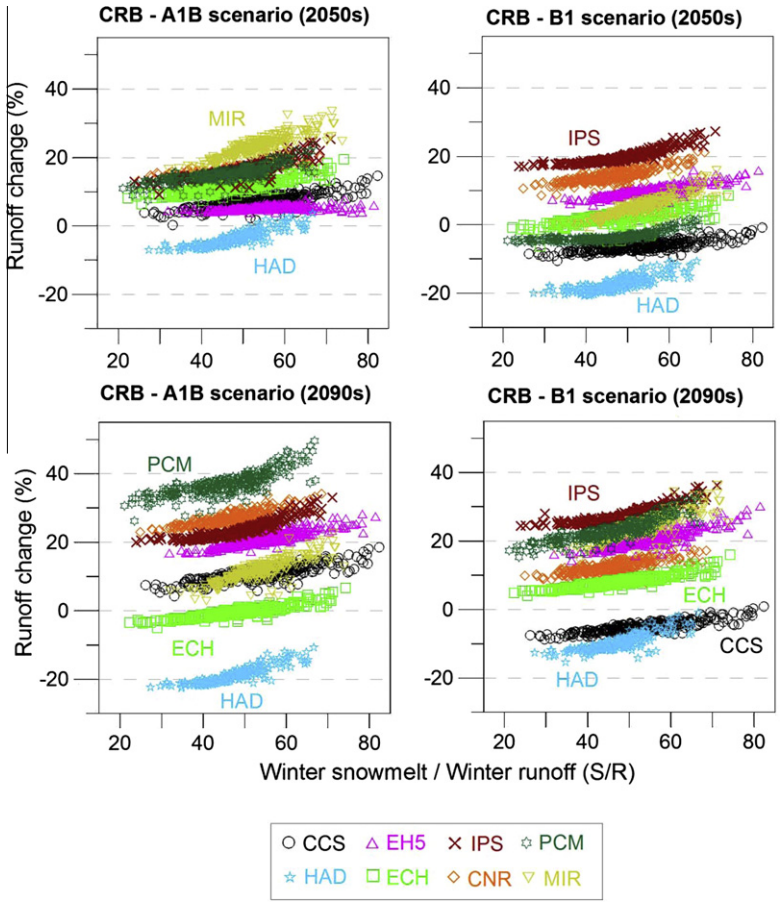

Fig. 13. Relationship of ratio of winter snowmelt to winter runoff (S/R) for reference period and change in winter runoff for 2050s and 2090s periods, here, the individual markers indicate the PRMS runs with 300 parameter sets.

snow-dominated basin (the CRB) is more dependent on the hydrologic parameters; they have less influence in the rainfall-dominated basin (the TRB). This result indicates that climate change impact assessment in snowfall-dominated regions may require more caution in runoff projection interpretation and more reliability in hydrologic model selection and parameter estimation (Moradkhani and Sorooshian, 2008; Najafi et al., 2011b).

Estimated hydrological model parameters may depend on calibration conditions (Merz et al., 2011; Peel and Blöschl, 2011). This study used different calibration periods in CRB (1973–1983) and TRB (1973–2006) given the availability of observed flow data. However, the distributions of calibrated parameters in both regions are similar, except *soil2gw_max* and *tmax_allsnow* (Fig. 4). In general, given the importance of uncertainty arising from hydrologic model parameters, caution needs to be taken by identifying sensitive parameters for calibration.

Downscaling methods and hydrologic model structures are also important uncertainty sources. Previous studies (Wilby and Wigley, 1997; Wood et al., 2004; Fowler et al., 2007; Im et al., 2010; Najafi et al., 2011a) report that different downscaling methods—statistical downscaling and dynamical downscaling—can create an additional source of uncertainty. Different hydrologic models that have different model assumptions could introduce yet another source of uncertainty. However, dealing with uncertainties associated with downscaling methods and hydrologic model structure selection is beyond the scope of this study and for further detail we refer the reader to studies conducted by Najafi et al. (2011a,b).

5.2. Cause of uncertainty in winter flow change

If the quantification and propagation of uncertainty sources are possible through further research or modeling improvement, the uncertainty associated with climate change impacts will be potentially reduced (IPCC, 2007). To investigate the cause of larger uncertainty from the hydrologic parameter in the CRB (winter flow in Fig. 9), a ratio of winter snowmelt to winter runoff (S/R) was estimated (see Fig. 12). The S/R represents the sensitivity of using hydrologic model parameter sets to precipitation and temperature changes on winter snowmelt. Lower S/R value can be less sensitive to temperature change than higher S/R value under the same precipitation change. Therefore, higher S/R value as a result of hydrologic model parameter uncertainty can induce higher change in the winter flow (see Fig. 13). Fig. 13 shows the significant relationship between the S/R value and winter runoff change; the Pearson correlation coefficients range from 0.79 to 0.90 for A1B and from 0.70 to 0.90 for B1 in the 2090s with 0.01 significance level. Also, the S/R values above 40% show steeper change in runoff than those below 40% S/R values. This result indicates that different sensitivity of hydrologic model parameter sets to climate change can cause hydrologic model uncertainty in snow-dominated regions such as CRB. Consequently, improving the accuracy of a snow process in hydrologic modeling could be of paramount importance in reducing the hydrologic uncertainty in snow-dominated regions. This will result in more reliable decisions on adaptation and mitigation strategies in the face of many uncertainties about future hydrologic projections.

6. Summary and conclusions

In this study, we examined various sources of uncertainty in hydrologic climate change impact assessment for both rain-dominated and snow-dominated basins. This study investigated the relative contribution of uncertainty sources, including GCM, GHG emission scenario, and hydrologic parameters. Eight GCMs were used to represent GCM model uncertainty and two GHG emission scenarios were used to represent the future range of projected GHG emission. The uncertainty from PRMS model parameters was represented by selecting behavioral parameters using Latin Hypercube Sampling (LHS), used to sample the hydrologic model parameters. The important results drawn from this study are summarized as follows.

(1) Hydrologically distinct river basins may have different ranges of uncertainty in climate impact study. Especially, changes in winter runoff are more affected by hydrologic parameter uncertainty in a snow-dominated basin, while these changes are less pronounced in a rain-dominated basin.
(2) The differences of uncertainty between the two basins stem from snow modeling. The results suggest that climate change impact assessment in snow-dominated regions would require more caution in interpreting future runoff projections because of the uncertainty of modeling snowmelt.
(3) The uncertainty in runoff change varies with time and between the basins, although some of this is due to the relatively higher uncertainty ranges of temperature and precipitation changes at the end of the 21st century. Because the ranges of GHG emission scenarios used in this study do not cover the full IPCC SRES range, further studies seem necessary for a more complete assessment of uncertainty related to emission scenarios.

There are several sources of uncertainty to be considered in hydrologic climate change impact assessment. This study did not discuss other sources of uncertainties, including downscaling method Najafi et al. (2011a), hydrologic model structure Najafi et al. (2011b), and GCM initial conditions. While including these sources may shift the relative contributions of the uncertainty sources, GCM structural uncertainty is still likely to be the biggest source of uncertainty as reviewed by Praskievicz and Chang (2009a). The direction and magnitude of future precipitation and temperature changes substantially vary among different GCMs, particularly at a regional scale. Further studies are underway to quantify the relative contribution of all uncertainty sources to runoff changes.

Acknowledgements

This research was partially supported by James F. and Marion L. Miller foundation and Institute for Sustainable Solutions (ISS) at Portland State University. We thank you Madeline Steele of Portland State University for proofreading the manuscript. The manuscript was greatly improved by the valuable comments from two anonymous reviewers.

References

Bae, D.H., Jung, I.W., Chang, H., 2008a. Potential changes in Korean water resources estimated by high-resolution climate simulation. Clim. Res. 35, 213–226.
Bae, D.H., Jung, I.W., Chang, H., 2008b. Long-term trend of precipitation and runoff in Korean river basins. Hydrol. Process. 22, 2644–2656.
Bae, D.H., Jung, I.W., Lettenmaier, D.P., 2011. Hydrologic uncertainties in climate change from IPCC AR4 GCM simulations of the Chungju Basin, Korea. J. Hydrol. 401 (1–2), 90–105.
Bates, B., Kundzewicz, Z.W., Wu, S., Palutikof, J.P., Eds., 2008. Climate Change and Water. Technical Paper of the Intergovernmental Panel on Climate Change (IPCC), Geneva, pp. 1–210.
Burlando, P., Rosso, R., 2002. Effects of transient climate change on basin hydrology. 1. Precipitation scenarios for the Arno River, central Italy. Hydrol. Process. 16, 1151–1175.
Chang, H., 2007. Comparative streamflow characteristics in urbanizing basins in the Portland Metropolitan Area, Oregon, USA. Hydrol. Process. 21 (2), 211–222.
Chang, H., Jung, I.W., 2010. Spatial and temporal changes in runoff caused by climate change in a complex large river basin in Oregon. J. Hydrol. 388, 186–207.
Choi, H.T., Beven, K., 2007. Multi-period and multi-criteria model conditioning to reduce prediction uncertainty in an application of TOPMODEL within the GLUE framework. J. Hydrol. 332, 316–336.
Collins, W., Bitz, C., Blackmon, M., Bonan, G., Bretherton, C., Carton, J., Chang, P., Doney, S., Hack, J., Henderson, T., Kiehl, J., Large, W., McKenna, D., Santer, B., Smith, R., 2006. The community climate system model version 3 (CCSM3). J. Clim. 19, 2122–2143.
Dagnachew, L., Christine, V.C., Francoise, G., 2003. Hydrological response of a catchment to climate 642 and land use changes in tropical Africa: case study South Central Ethiopia. J. Hydrol. 275, 67–85.
Davey, K.R., 2008. Latin hypercube sampling and pattern search in magnetic field optimization problems. IEEE Trans. Magn. 44 (6), 974–977.
Dressler, K.A., Leavesley, G.H., Bales, R.C., Fassnacht, S.R., 2006. Evaluation of gridded snow water equivalent and satellite snow cover products for mountain basins in a hydrologic model. Hydrol. Process. 20, 673–688.
Federer, C.A., Vörösmarty, C., Fekete, B., 1996. Intercomparison of methods for calculating potential evaporation in regional and global water balance models. Water Resour. Res. 32, 2315–2321.
Fegeas, R.G., Claire, R.W., Guptill, S.C., Anderson, K.E., Hallam, C.A., 1983. Land Use and Land Cover Digital Data: US Geological Survey Circular 895-E, 30 p.
Fowler, H.J., Blenkinsop, S., Tebaldi, C., 2007. Linking climate change modeling to impacts studies: recent advances in downscaling techniques for hydrological modeling. Int. J. Climatol. 27, 1547–1578.
Franczyk, J., Chang, H., 2009. The effects of climate change and urbanization on the runoff of the Rock Creek in the Portland metropolitan area, OR, USA. Hydrol. Process. 23, 805–815.
Freer, J., Beven, K., Ambroise, B., 1996. Bayesian estimation of uncertainty in runoff prediction and the value of data: an application of the GLUE approach. Water Resour. Res. 32 (7), 2161–2173.
Gordon, C., Cooper, C., Senior, C., Banks, H., Gregory, J., Johns, T., Mitchell, J., Wood, R., 2000. The simulation of SST, sea ice extents and ocean heat transports in a version of the Hadley Centre coupled model without flux adjustments. Clim. Dyn. 16, 147–168.
Graves, D., Chang, H., 2007. Hydrologic impacts of climate change in the Upper Clackamas basin of Oregon. Clim. Res. 33 (2), 143–157.
Halmstad, A., Najafi, M.R., Moradkhani, H., 2012. Analysis of precipitation extremes with the assessment of regional climate models over the Willamette River Basin, USA. Hydrol. Process.. http://dx.doi.org/10.1002/hyp.9376.
Hamon, W.R., 1961. Estimating potential evapotranspiration. Proc. Am. Soc. Civil Eng., J. Hydraul. Div. 87, 107–120.
Hawkins, E., Sutton, R., 2009. The potential to narrow uncertainty in regional climate predictions. Bull. Am. Meteorol. Soc. 90 (8), 1095–1107.
Hay, L.E., Clark, M.P., 2003. Use of statistically and dynamically downscaled atmospheric model output for hydrologic simulations in three mountainous basins in the western United States. J. Hydrol. 282, 56–75.
Hay, L.E., Leavesley, G.H., Clark, M.P., Markstrom, S.L., Viger, R.J., Umemoto, M., 2006. Step-wise, multiple-objective calibration of a hydrologic model for a snowmelt-dominated basin. J. Am. Water Resour. Assoc. 42, 877–890.
Hay, L.E., McCabe, G.J., Clark, M.P., Risley, J.C., 2009. Reducing streamflow forecast uncertainty: application and qualitative assessment of the upper Klamath river basin, Oregon. J. Am. Water Resour. Assoc. 45, 580–596.
Im, E.S., Jung, I.W., Chang, H., Bae, D.H., Kwon, W.T., 2010. Hydroclimatological response to dynamically downscaled climate change simulations for Korean basins. Clim. Change 100, 485–508.
Iman, R.L., Helton, J.C., Campbell, J.E., 1981. An approach to sensitivity analysis of computer models. Part 1. Introduction, input variable selection and preliminary variable assessment. J. Qual. Technol. 13 (3), 174–183.
IPCC (Intergovernmental Panel on Climate Change), 2000. Special Report on Emission Scenarios (SRES): A Special Report of Working Group III of the Intergovernmental Panel on Climate Change. Cambridge University Press, Cambridge.
IPCC (Intergovernmental Panel on Climate Change), 2007. Climate Change 2007: The Scientific Basis, IPCC Contribution of Working Group I to the Fourth Assessment Report of the Intergovernmental Panel on Climate Change. Cambridge University Press, Cambridge.
Jiang, T., Chen, Y.D., Xu, C., Chen, X., Chen, X., Singh, V.P., 2007. Comparison of hydrological impacts of climate change simulated by six hydrological models in the Dongjiang Basin, South China. J. Hydrol. 336, 316–333.
Jungclaus, J.H., Botzet, M., Haak, H., Keenlyside, N., Luo, J., Latif, M., Marotzke, J., Mikolajewicz, U., Roeckner, E., 2006. Ocean circulation and tropical variability in the coupled model ECHAM5/MPI-OM. J. Clim. 19, 3952–3972.

Jung, I.W., Chang, H., 2011. Assessment of future runoff trends under multiple climate change scenarios in the Willamette River Basin, Oregon, USA. Hydrol. Process. 25, 258–277.
Jung, I.W., Chang, H., Moradkhani, H., 2011. Quantifying uncertainty in urban flooding analysis considering hydro-climatic projection and urban development effects. Hydrol. Earth Syst. Sci. 15, 617–633.
Kay, A.L., Davies, H.N., Bell, V.A., Jones, R.G., 2009. Comparison of uncertainty sources for climate change impact: flood frequency in England. Clim. Change 92, 41–63.
Kleinen, T., Petschel-Held, G., 2007. Integrated assessment of changes in flooding probabilities due to climate change. Clim. Change 81, 283–312.
K-1 Model Developers, 2004. K-1 coupled model (MIROC) description. In: Hasumi, H., Emori, S. (Eds.), K-1 Technical Report 1: Center for Climate System Research. University of Tokyo, 34pp. <http://www.ccsr.u-tykyo.ac.jp/kyosei/hasumi/MIROC/tech-repo.pdf>.
Laenen, A., Risley, J.C., 1997. Precipitation–Runoff and Streamflow-Routing Models for the Willamette River Basin, Oregon. US Geological Survey Water-Resources Investigations, Report 95-4284.
Leavesley, G.H., Lichty, R.W., Troutman, B.M., Saindon, L.G., 1983. Precipitation Runoff Modeling System: User's Manual. US Geological Survey Water Resources Investigation Report, pp. 83–4238.
Leavesley, G.H., Markstrom, S.L., Restrepo, P.J., Viger, R.J., 2002. A modular approach to addressing model design, scale and parameter estimation issues in distributed hydrological modeling. Hydrol. Process. 16, 173–187.
Leavesley, G.H., Stannard, L.G., 1995. The precipitation–runoff modeling system – PRMS. In: Singh, V.P. (Ed.), Computer Models of Watershed Hydrology. Water Resources Publications, Highlands Ranch, Colorado, pp. 281–310 (Chapter 9).
Madadgar, S., Moradkhani, H., in press. Drought analysis under climate change using copula. J. Hydrol. Eng. http://dx.doi.org/10.1061/(ASCE)HE.1943-5584.0000532.
Marti, O., Bracommot, P., Bellier, J., Benshila, R., Bony, S., Brockmann, P., Cadulle, P., Caubel, A., Denvil, S., Dufresne, J., Fairhead, L., Filiberti, M., Hourdin, F., Krinner, G., Levy, C., Musat, I., Talandier, C., 2005. The New IPSL Climate System Model: IPSL-CM4. Institut Poerre Simon Laplace des Sciences del'Environnement Global. <http://dods.ipsl.jussieu.fr/omamce/IPSLCM4/>
McFarland, W.D., 1983. A Description of Aquifer Units in Western Oregon. US Geological Survey Open-File Report 82-165, 35 p.
McKay, M.D., Beckman, R.J., Conover, W.J., 1979. A comparison of three methods for selecting values of input variables in the analysis of output from a computer code. Technometrics 21 (2), 239–245.
Merz, R., Parajka, J., Blöschl, G., 2011. Time stability of catchment model parameters: implications for climate impact analyses. Water Resour. Res. 47, W02531. http://dx.doi.org/10.1029/2010WR009505.
Min, S.K., Legutke, S., Hense, A., Kwon, W.T., 2005. Internal variability in a 1000-year control simulation with the coupled climate model ECHO-G. Part I. Near-surface temperature, precipitation and sea level pressure. Tellus 57A, 605–621.
Moradkhani, H., Meier, M., 2010. Long-lead water supply forecast using large-scale climate predictors and independent component analysis. J. Hydrol. Eng. 15 (10), 744–762. http://dx.doi.org/10.1061/(ASCE)HE.1943-5584.0000246.
Moradkhani, H., Baird, R.G., Wherry, S., 2010. Assessment of climate change impact on floodplain and hydrologic ecotones. J. Hydrol. 395 (3–4), 264–278.
Moradkhani, H., Sorooshian, S., 2008. General review of rainfall–runoff modeling: model calibration, data assimilation, and uncertainty analysis, in hydrological modeling and water cycle, coupling of the atmospheric and hydrological models. Water Sci. Technol. Libr. 63 (Part 1), 1–24. http://dx.doi.org/10.1007/978-3-540-77843-1_1.
Najafi, M.R., Moradkhani, H., Wherry, S.A., 2011a. Statistical downscaling of precipitation using machine learning with optimal predictor selection. J. Hydrol. Eng. 16 (8), 650–664. http://dx.doi.org/10.1061/(ASCE)HE.1943-5584.0000355.
Najafi, M.R., Moradkhani, H., Jung, I.W., 2011b. Assessing the uncertainties of hydrologic model selection in climate change impact studies. Hydrol. Process. 25 (18), 2814–2826.
Nash, J.E., Sutcliffe, J.V., 1970. River flow forecasting through conceptual models part I – a discussion of principles. J. Hydrol. 10 (3), 282–290.
NOAA COOP (National Oceanic and Atmospheric Administration Cooperative Observer Program). <http://www.nws.noaa.gov/om/coop>.
NRCS (Natural Resources Conversation Service), 1986. General Soil Map, State of Oregon: Portland, Oregon, Natural Resource Conservation Service, Scale 1:1,000,000.
NRCS SNOTEL (Natural Resources Conversation Service Snow Telemetry System), 2011. <http://www.or.nrcs.usda.gov/snow/maps/oregon_sitemap.html>.
Obled, C., Rosse, B., 1977. Mathematical models of a melting snowpack at an index plot. J. Hydrol. 32, 139–163.
OCS (Oregon Climate Service), 2011. Precipitation Elevation Regressions on Independent Slopes Model (PRISM). <http://www.prism.oregonstate.edu/>.
Peel, M.C., Blöschl, G., 2011. Hydrological modeling in a changing world. Prog. Phys. Geogr. 35 (2), 249–261.
Poff, N.L., 1996. A hydrogeography of unregulated streams in the United States and an examination of scale-dependence in some hydrological descriptors. Freshwater Biol. 36, 71–91.
Praskievicz, S., Chang, H., 2009a. A review of hydrologic modeling of basin-scale climate change and urban development impacts. Prog. Phys. Geogr. 33, 650–671.
Praskievicz, S., Chang, H., 2009b. Winter precipitation intensity and ENSO/PDO variability in the Willamette Valley of Oregon. Int. J. Climatol. 29 (13), 2033–2039.
Praskievicz, S., Chang, H., 2011. Impacts of climate change and urban development on water resources in the Tualatin River basin, Oregon. Ann. Assoc. Am. Geogr. 101 (2), 249–271.
Prudhomme, C., Davies, H., 2008. Assessing uncertainties in climate change impact analyses on the river flow regimes in the UK. Part 2: future climate. Clim. Change 93, 197–222.
Risley, J., Moradkhani, H., Hay, L., Markstrom, S., 2011. Statistical comparisons of watershed-scale response to climate change in selected basins across the United States. AMS Earth Interact. 15 (14), 1–26.
Rounds, S.A., Wood, T.M., 2001. Modeling Water Quality in the Tualatin River, Oregon, 1991–1997. US Geological Survey Water-Resources Investigations, Report 01-4041.
Salathé Jr., E.P., 2005. Downscaling simulations of future global climate with application to hydrologic modeling. Int. J. Climatol. 25, 419–436.
Salathé Jr., E.P., Mote, P.W., Wiley, M.W., 2007. Review of scenario selection and downscaling methods for the assessment of climate change impacts on hydrology in the United States Pacific Northwest. Int. J. Climatol. 27, 1611–1621.
Shaw, S.B., Riha, S.J., 2011. Assessing temperature-based PET equations under a changing climate in temperature, deciduous forests. Hydrol. Process. 25 (9), 1466–1478.
Tague, C., Grant, G.E., 2004. A geological framework for interpreting the low-flow regimes of Cascade streams, Willamette River Basin, Oregon. Water Resour. Res. 40, W04303. http://dx.doi.org/10.1029/2003WR002629.
Tague, C., Grant, G., Farrell, M., Choate, J., Jefferson, A., 2008. Deep groundwater mediates streamflow response to climate warming in the Oregon Cascades. Clim. Change 86, 189–210.
Tebaldi, C., Smith, R.L., Nychka, D., Mearns, L.O., 2005. Quantifying uncertainty in projections of regional climate change: a Bayesian approach to the analysis of multimodel ensembles. J. Clim. 18, 1524–1540.
Terray, L., Valcke, S., Piacentini, A., 1998. Oasis 2.2 Ocean Atmosphere Sea Ice Soil, User's Guide and Reference Manual, Technical Report TR/CMGC/98-05. CERFACS, Toulouse, France.
USGS NWIS (US Geological Survey National Water Information System), 2011. USGS Surface-Water Statistics for Oregon. <http://waterdata.usgs.gov/or/nwis/> (accessed 12.10.09).
USGS (US Geological Survey), 1990. Digital Elevation Models: US Geological Survey, National Mapping Program, Technical Instructions Data User Guide 5, 51 p.
Vörösmarty, C.J., Federer, C.A., Schloss, A.L., 1998. Potential evaporation functions compared on US watersheds: possible implications for global-scale water balance and terrestrial ecosystem modeling. J. Hydrol. 207, 147–169.
Washington, W., Weatherly, J., Meehl, G., Semtner, A., Bettge, T., Craig, A., Strand, W., Arblaster, J., Wayland, V., James, R., Zhang, Y., 2000. Parallel climate model (PCM) control and transient simulations. Clim. Dyn. 16, 755–774.
Wilby, R.L., 2005. Uncertainty in water resource model parameters used for climate change impact assessment. Hydrol. Process. 19, 3201–3219.
Wilby, R.L., Harris, I., 2006. A framework for assessing uncertainties in climate change impacts: low-flow scenarios for the River Thames, UK. Water Resour. Res. 42, W02419. http://dx.doi.org/10.1029/2005WR004065.
Wilby, R.L., Wigley, T.M.L., 1997. Downscaling general circulation model output: a review of methods and limitations. Prog. Phys. Geogr. 21, 530–548.
Wilby, R.L., Whitehead, P.G., Wade, A.J., Butterfield, D., Davis, R.J., Watts, G., 2006. Integrated modelling of climate change impacts on water resources and quality in a lowland catchment: River Kennet, UK. J. Hydrol. 330, 204–220.
Wood, A.W., Leung, L.R., Sridhar, V., Lettenmaier, D.P., 2004. Hydrologic implications of dynamical and statistical approaches to downscaling climate model outputs. Clim. Change 62, 189–216.
Wood, A.W., Maurer, E.P., Kumar, A., Lettenmaier, D.P., 2002. Long-range experimental hydrologic forecasting for the eastern United States. J. Geophys. Res. – Atmos. 107, 4429–4443.